RESEARCH PAPER

An easy method for assessing frost susceptibility of soils: the freezing ring test

Jiazuo Zhou[1] · Wansheng Pei[2,3] 🔘 · Xiyin Zhang[4] · Wanlin Liu[1,5] · Changfu Wei[1,3]

Abstract

Frost heave induces deformation and damage to various facilities in cold regions and on artificially frozen ground. A convenient and quick way to assess frost susceptibility is favorable to deal with frost heave. This study introduced an easy freezing ring test, in which a short cylindrical soil sample is frozen from the outmost boundary to its center with thermal isolation on its top and bottom. During freezing, water migrates from the center to the outer zone in the same direction as heat transfer. Water content along the radial direction was measured after the freezing test. Soil types, initial water content, and salt concentration were considered as influencing factors for water migration. Then, water redistribution by the freezing ring test was compared with the frost heave tests, showing a good agreement in water migration and frost heave capabilities. An index of water redistribution by the freezing ring test was suggested to assess frost susceptibility. The frost susceptibility is high in silt, very low to medium in clay, and negligible in sand. Increased initial water content aggravates frost heave but salt significantly depresses it. The freezing ring test is easy and time-saving to conduct; thus, it is potentially suitable for large engineering projects.

1 Introduction

Frost heave, a phenomenon of ground uplift due to soil freezing and swelling, occurs when the ground temperature falls below its freezing point. Frost heave is very common in cold regions, posing a risk to the stability of railways [1, 24], highways [33], pipelines [26], and airports [21] on

✉ Wansheng Pei
  peiwansheng@lzb.ac.cn

1 State Key Laboratory of Geomechanics and Geotechnical Engineering, Institute of Rock and Soil Mechanics, Chinese Academy of Sciences, Wuhan, Hubei, China

2 State Key Laboratory of Frozen Soil Engineering, Northwest Institute of Eco-Environment Resources, Chinese Academy of Sciences, Lanzhou, Gansu, China

3 University of Chinese Academy of Sciences, Beijing, China

4 School of Civil Engineering, Lanzhou Jiaotong University, Lanzhou, Gansu, China

5 Guangxi Key Laboratory of Geomechanics and Geotechnical Engineering, Guilin University of Technology, Guilin 541004, China

the frozen ground. The artificial ground freezing method could be adopted as a supporting technique for underground works through water-rich and soft soil layers for its efficiency in preventing water flow and enhancing soil strength [19, 22, 30]. However, potential frost heave may induce deformation to infrastructure above the artificially frozen area. Knowledge of frost susceptibility is essential to estimate the soil behavior under frost heave and to present solution strategies.

When water turns into ice on freezing, its volume expands by about 9%. This water–ice volume expansion induces the in situ frost heave, where water is assumed to freeze in the pores without flowing [13]. The in situ frost heave is minor when the porosity, water saturation, and unfrozen water content are considered. Ice segregation and water migration are other causes of frost heave [15, 37, 43, 44]. During soil freezing, discrete ice lenses form and separate soil particles so that soil expands greatly. Meanwhile, cryogenic suction near the freezing front draws water from the unfrozen zone to continuously feed the growing ice lens. In most cases, ice segregation has the highest contribution to the frost heave. Vapor transfer may

play an essential role in frost heave in unsaturated soils [4, 38, 39], where water migration is less significant due to its low hydraulic conductivity.

Quite a few researchers have presented various methods to assess frost susceptibility, theoretically, experimentally, and empirically during the past decades. Many theories have been developed to address the physics of frost heaves, such as the primary heave model [11, 28], secondary heave model [12, 23, 25, 28], segregation potential theory [16, 17], and premelting dynamics [31, 35, 41]. Although interesting, it is not easy for engineers to solve theoretical models that include a group of partial differential equations of water and heat transfer and soil deformation. The frost heave test directly measures frost heave in the laboratory. Such a test is usually conducted on a soil column with unidirectional freezing in one dimension to model the real freezing process of natural ground [3, 27, 36, 45]. However, conducting a frost heave test is complicated and time-consuming, limiting its application to large projects. For practical purposes, engineers have suggested various classification systems for frost susceptibility according to soil properties that could be easily obtained. The classification criterion could be based on the soil particle size [2, 5, 9], plasticity [6, 7, 9, 40], or permeability [32]. Unfortunately, the classification is undoubtedly too empirical to be applied to various soils and environmental conditions.

As mentioned above, water migration is highly associated with frost heave, so the water redistribution in frozen soil may be taken as an indicator of frost susceptibility. Therefore, this study introduced an easy freezing ring test to quantify the water migration during soil freezing. The water redistribution characteristics were analyzed theoretically and compared with the results of direct frost heave tests. Based on the experimental and theoretical results, frost susceptibility was classified by the index of water redistribution. Since the freezing ring test is easier than the traditional frost heave test, it is potentially suitable for large projects that require a great number of tests to be completed.

2 Experimental methods and materials
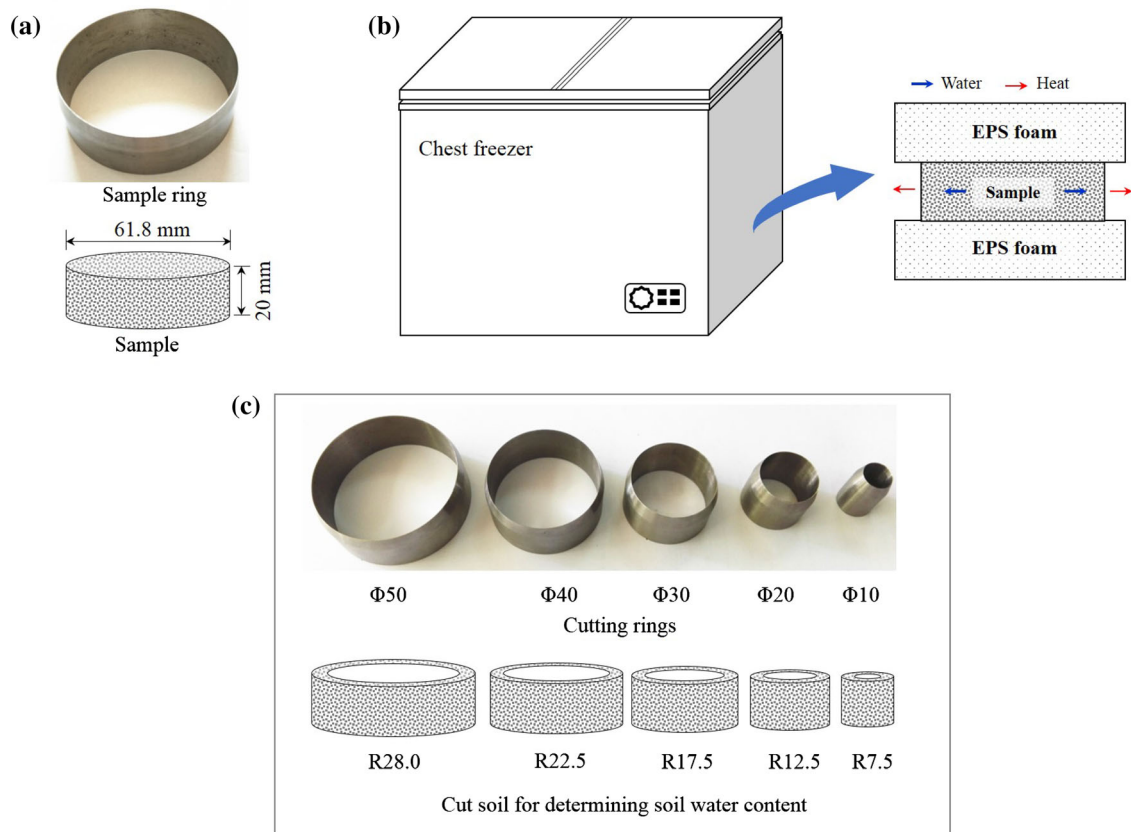
2.1 Freezing ring test

To prepare soil specimens with moisture content and salt concentration, salt was initially dissolved in distilled water. Subsequently, the solution with the specified concentration was added to dry soil. Herein, sodium chloride (NaCl) is adopted as the salt component owing to its very low eutectic point with soil water ($< - 21$ °C), ensuring that it stays dissolved even in the frozen soil. In the specimens with salt, the water content is simplified as the ratio of

solution mass (including salt and water) to dry soil mass. In the specimens without salt, only water was added to the dry soil. Subsequently, the soil was transferred to a cylindrical mold with a steel ring at the bottom. To shape the sample, the soil in the cylindrical mold was compressed by a steel column into the steel ring, with an inner diameter of 61.8 mm and a height of 20 mm (Fig. 1a). Then, the short cylindrical soil sample and the ring were sandwiched between two pieces of expanded polystyrene (EPS) foam for vertical thermal insulation. After that, the sample with EPS foam was placed in a chest freezer for cooling. During the sample cooling, heat was extracted from the sidewall so that the sample gradually freezes from the outer to the inner zone (Fig. 1b). Cryogenic suction due to freezing drew the water in the inner zone to near the freezing front and turned into ice. As the freezing front moved to the sample center, the total water (ice and water) content increased in the outer zone but decreased in the inner zone. The cooling duration lasted for 6 h to ensure that the sample was completely frozen. Following that, the frozen soil sample was removed from the sample ring. Another cutting ring with a diameter of 50 mm was used to cut the soil sample into two parts: a smaller soil sample with a diameter of 50 mm and a soil layer with an average radius of 28.0 mm (outer diameter of 61.8 mm and inner diameter of 50 mm). Repeating the cutting procedures with different cutting rings whose diameters range from 40 to 10 mm, one can obtain the soil at different radii, ranging from 22.5 to 7.5 mm (Fig. 1c). Consequently, the water content in the cut soil was determined using the oven drying method. In this way, the water content distribution along the radial direction could be obtained.

To investigate the temperature field inside the sample, a numerical simulation was conducted. Due to the axisymmetry of the freezing ring test, only half of the geometrical model is needed (Fig. 2a). In the simulation, the difference in the thermal properties between frozen and unfrozen soil is ignored. The phase change is assumed to occur from 0 to $- 0.4$ °C, and water migration is ignored. The simulated results show that the temperature in the vertical direction varies negligibly in the soil sample (Fig. 2b, c), indicating that the insulating EPS foam makes the heat in the soil only transfer in the radial direction. Although simplified, the simulation provides a schematic of the temperature fields in the freezing sample.

2.2 Frost heave test

The frost heave test was conducted in an axial freezing apparatus (Fig. 3). The soil sample with a diameter of 100 mm and a height of 100 mm was placed in a sample cell which was made of plexiglass. The top and bottom of the sample were touched by two metal plates. Cooling
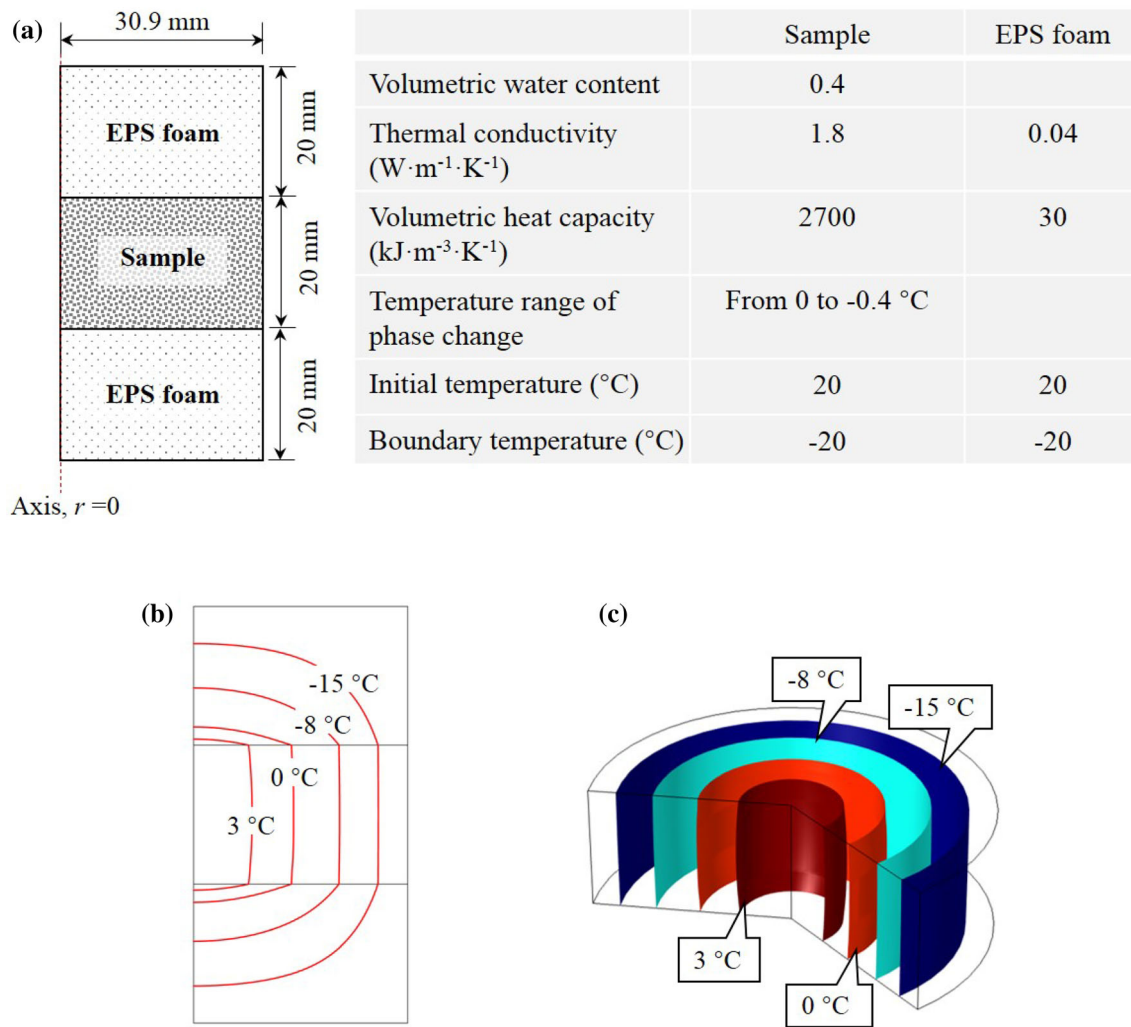
Fig. 1 Procedure of freezing ring test. **a** Packing soil in the sample ring; **b** Freezing the soil sample in a chest freezer; **c** Using cutting rings with diameters from 50 to 10 mm to cut the soil sample into layers with radii ranging from 28.0 mm to 7.5 mm. Φ denotes the diameter of cutting rings in millimeter; R denotes the average radius of the soil layer in millimeter

liquid circulated through the metal plates and water baths to control the boundary temperatures for the sample. The sample cell was coated with thermal insulation foam to eliminate the radial heat flux and ensure heat transfers in the axial direction. The top plate was fixed to a loading rod connected to the reaction frame. The bottom place was fixed to another loading rod, which can be driven upward or downward by an actuating motor. The entire testing apparatus was placed in a cooling chamber. During the freezing, the temperature in the cooling chamber was set at 1 °C; the top plate temperature was lower than the soil freezing point; the bottom plate temperature was higher than the soil freezing point. Resistance thermometers spacing 10 mm were inserted into the sample and plates to monitor the temperature. A water source outside the cooling chamber supplies water through a tube connected to the bottom plate. In this way, the soil sample was frozen from top to bottom, and water was drawn through the bottom plate and unfrozen zone to the frozen zone. Due to the frost heave, the soil sample expanded and pushed the bottom plate downward. Each test lasted for about 10 h. After the test, soil slices with a thickness of 10 mm were cut along the sample height. The total water content of these slices was measured using the oven drying method, from which water redistribution could be obtained.

2.3 Testing materials

In this study, three types of soils were selected: a clay obtained from Sanmenxia, Henan Province, China, a silt from Zhengzhou, Henan Province, China, and the China ISO standard sand that pass through 0.5 mm sieve. The particle size distribution curve was determined by sieve analysis for the sand and by the hydrometer method for the silt and clay (Fig. 4). The specific gravity is 2.65, 2.72, and 2.74 for sand, silt, and clay, respectively. The liquid and plastic limits are 36.2 and 19.4, respectively, for clay, and 27.5 and 15.5, respectively, for silt. The boundary temperature, initial water content, and salt concentration are also considered in the tests, as presented in Tables 1 and 2. Besides the tests presented in Table 1, an additional freezing ring test was conducted on the silt sample with a plastic film ring inserted at a radius of 25 mm to stop water migration.

(a)

		Sample	EPS foam
	Volumetric water content	0.4	
	Thermal conductivity (W·m⁻¹·K⁻¹)	1.8	0.04
	Volumetric heat capacity (kJ·m⁻³·K⁻¹)	2700	30
	Temperature range of phase change	From 0 to -0.4 °C	
	Initial temperature (°C)	20	20
	Boundary temperature (°C)	-20	-20

(b)

(c)

Fig. 2 Numerical simulation of temperature distribution in the freezing ring test. **a** An axisymmetric geometry model for the freezing test. **b** Simulated isothermal curves in both the soil sample and EPS foam at 0.5 h. **c** 3-D isothermal surfaces inside the sample at 0.5 h

3 Experimental results

3.1 Results of freezing ring tests

Figure 5 shows the result of freezing ring tests on silt with an initial water content of 24.9%. The data at the center ($r = 0$ mm) were excluded because the cut soil in the smallest cutting ring (Φ10 in Fig. 1c) is too small to accurately determine its water content. As the soil with initial water content was fully blended before sample preparation, initial water content is assumed to be distributed uniformly in the entire sample. After freezing, water increased significantly in the outer zone but decreased in the inner zone. The significant water redistribution indicates that water migrates from the inner to the outer zone during freezing. When a plastic film ring was inserted into the soil at $r = 25$ mm to stop water migration, the water content outside the film ring approximated the

initial water content; however, water redistribution still occurred inside the film ring (Fig. 5a). The water migration coincides with the process of heat transfer from the inner to the outer zone. The tests under various boundary temperatures ranging from − 5 °C to − 20 °C show similar water redistribution (Fig. 5b), indicating that the cold boundary temperature is insignificant in the freezing ring tests. Hereinafter, all freezing ring tests were conducted at the boundary temperature of − 20 °C to investigate the impact of soil type, water content, and salt on water migration.

Figure 6 compares the results of water migration of clay, silt, and sand. Silt has the most significant water redistribution; clay has a weaker water redistribution than silt; sand does not show water redistribution as its water content change is within experimental error. For both clay and silt, a higher initial water content results in higher nonuniformity in the water content. The tendency in water
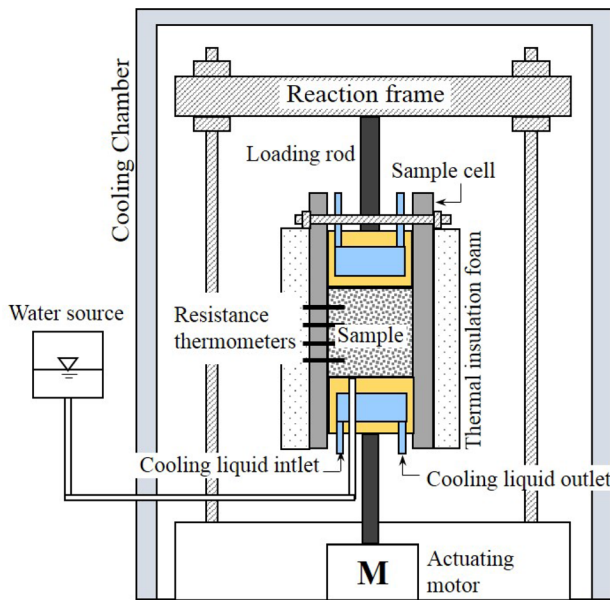
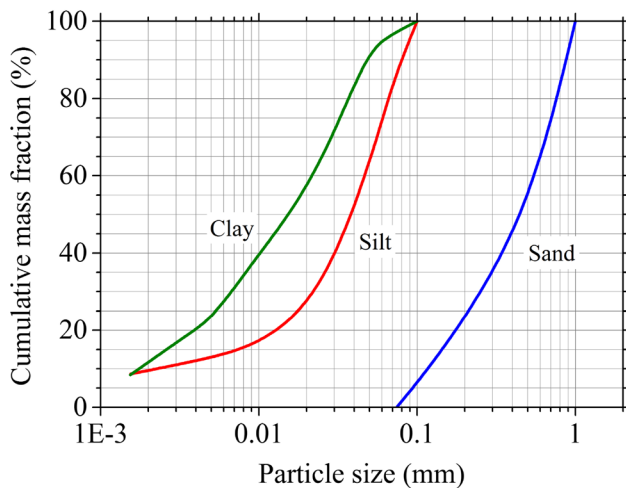**Fig. 3** Experimental configuration of frost heave

Fig. 4 Particle size distribution curves of the tested soils

Table 1 Test conditions for freezing ring tests

Soil type	Dry density (g/cm³)	Initial water content (%)	NaCl molarity (mol/L)	Cooling temperature (°C)
Clay	1.45	31.1	0.0	− 20
	1.45	31.7	0.5	− 20
	1.60	23.6	0.0	− 20
Silt	1.60	24.9	0	− 5
	1.60	24.9	0	− 10
	1.60	24.9	0	− 20
	1.60	24.0	0.5	− 20
	1.60	15.7	0	− 20
Sand	1.80	15.8	0	− 20
	1.80	13.0	0	− 20

At each condition, the test is conducted twice

Table 2 Test conditions for frost heave tests

Soil type	Dry density (g/cm³)	Initial water content (%)	NaCl molarity (mol/L)	Warm boundary (°C)	Cold boundary (°C)
Clay	1.45	32.0	0.0	3	− 3
	1.45	32.0	0.5	3	− 6
	1.60	24.0	0.0	3	− 3
Silt	1.60	25.0	0	3	− 3
	1.60	25.0	0.5	3	− 6
	1.60	16.0	0	3	− 3
Sand	1.80	13.0	0	3	− 3

At each condition, the test is conducted once. The overburden pressure is 6 kPa

redistribution qualitatively agrees with the frost suscepti-bility of soils. For a given soil, hydraulic conductivity and water retention capacity are two key properties that control water migration during freezing and consequently frost heave. The hydraulic conductivity controls the water migration in the unfrozen and partially frozen soil. The water retention capacity enables the frozen soil to hold some unfrozen water through which water penetrates into frozen soil. Significant water migration and frost heave only occur if the water pathways are free in both unfrozen and frozen soil. Generally, the soil retention capability negatively correlates with hydraulic conductivity. Sand has high hydraulic conductivity, but the unfrozen water film is too thin to allow water to penetrate into the frozen sand. Clay has a high water retention capability to hold

considerable unfrozen water; however, its hydraulic con-ductivity is very low and resists water migration. Silt has moderate hydraulic conductivity and water retention capacity, inducing the most significant water migration and frost heave. The initial water content affects water migra-tion by changing soil hydraulic conductivity.

The effect of salt on water migration was also investi-gated by adding 0.5 mol/L NaCl solution into the soil (Fig. 7). Although the initial water content is comparable, the nonuniformity in water redistribution is considerably weakened in salt-bearing soils in both clay and silt, indi-cating that salt resists water migration during freezing. A similar conclusion was made from previous frost heave tests, showing that salt suppresses frost heave [8, 10]. It is well known that salt can depress the soil freezing point by reducing the chemical potential of soil water. An intuitive idea is that the salt-induced freezing point depression reduces cryogenic suction, thus, weakening the water
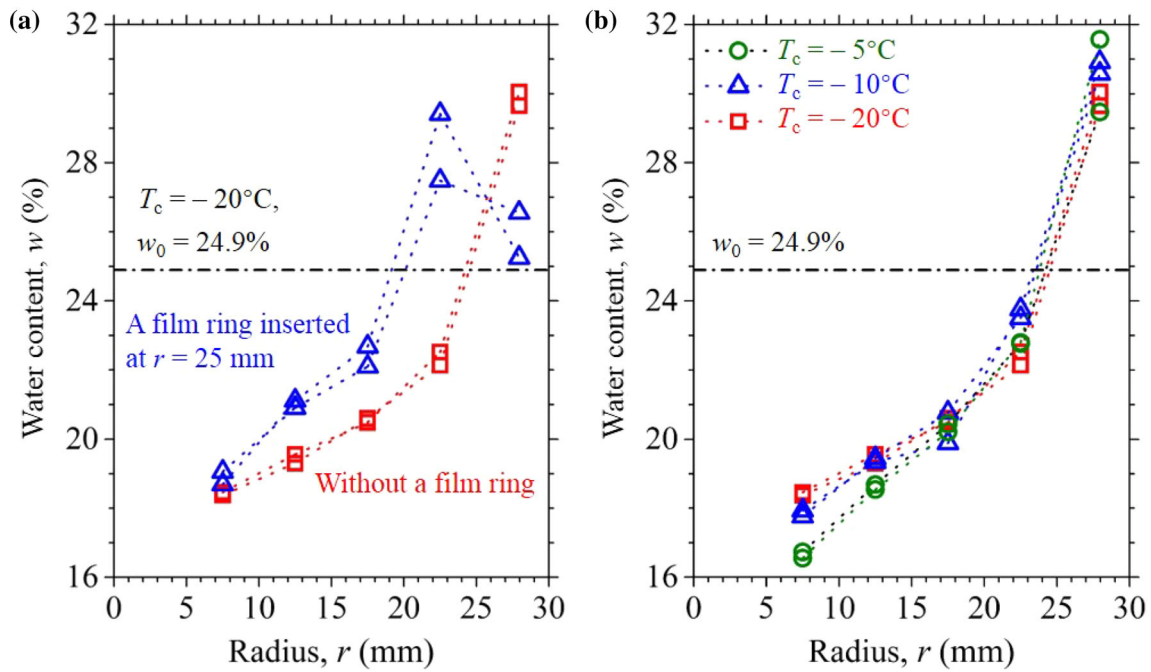
Fig. 5 Water redistribution of frozen silt in freezing ring tests with **a** a plastic film ring inserted at $r = 25$ mm and **b** various boundary temperatures. T_c is the boundary temperature (air temperature), and w_0 is the initial water content. Each test was conducted twice
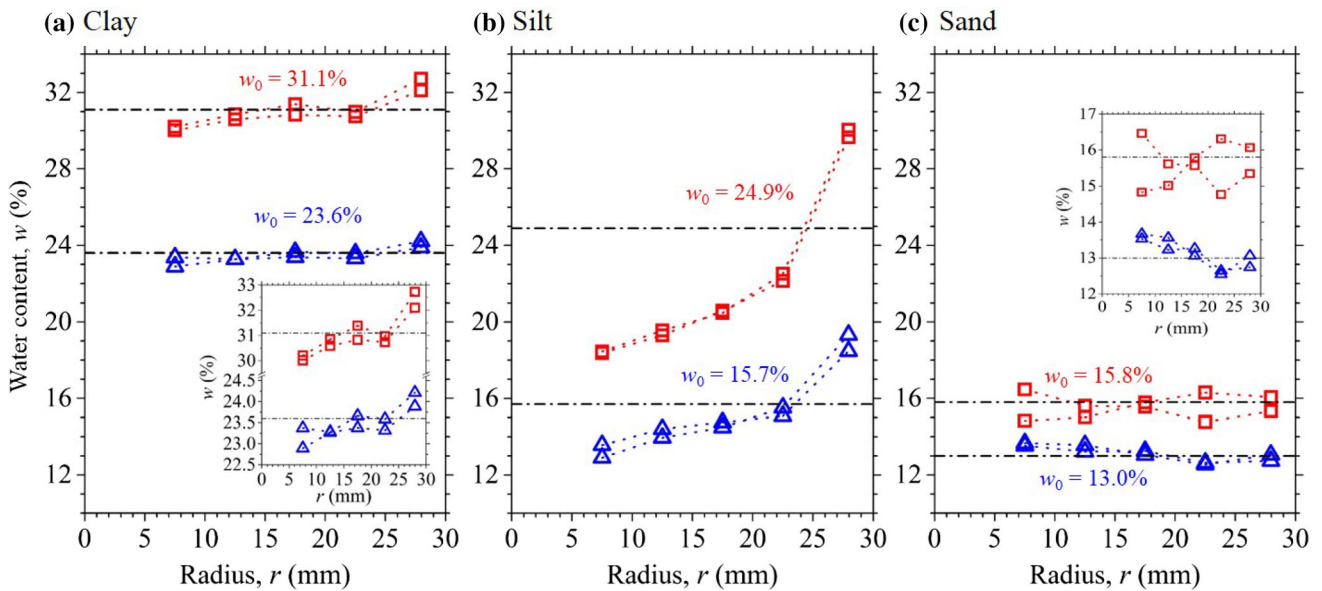
Fig. 6 Effect of soil type and initial water content on water redistribution. The insert graphs in (**a**) and (**c**) zoom in on the water redistribution

migration and frost heave. In an ideal solution, the freezing point depression coefficient is about 1.86 °C·L/mol. The freezing point of NaCl-bearing soil decreases similar to the ideal dilute solution when the ion molarity is less than 4 mol/L [46]. Thus, the freezing point of the soil containing 0.5 mol/L NaCl (1.0 mol/L ion, including Na$^+$ and Cl$^-$) is 1.86 °C lower than that of salt-free soil. Let us compare the tests on salt-free silt with a boundary

temperature of − 5 °C (Fig. 5b) and the NaCl-bearing silt with a boundary temperature of − 20 °C (Fig. 7b). The difference in the boundary temperature is 15 °C, larger than the salt-induced freezing point depression of 1.86 °C. However, water migration in the salt-bearing silt is still much weaker than that in the salt-free silt. The comparison result shows that the salt-induced freezing point depression may not be the true mechanism for restraining water
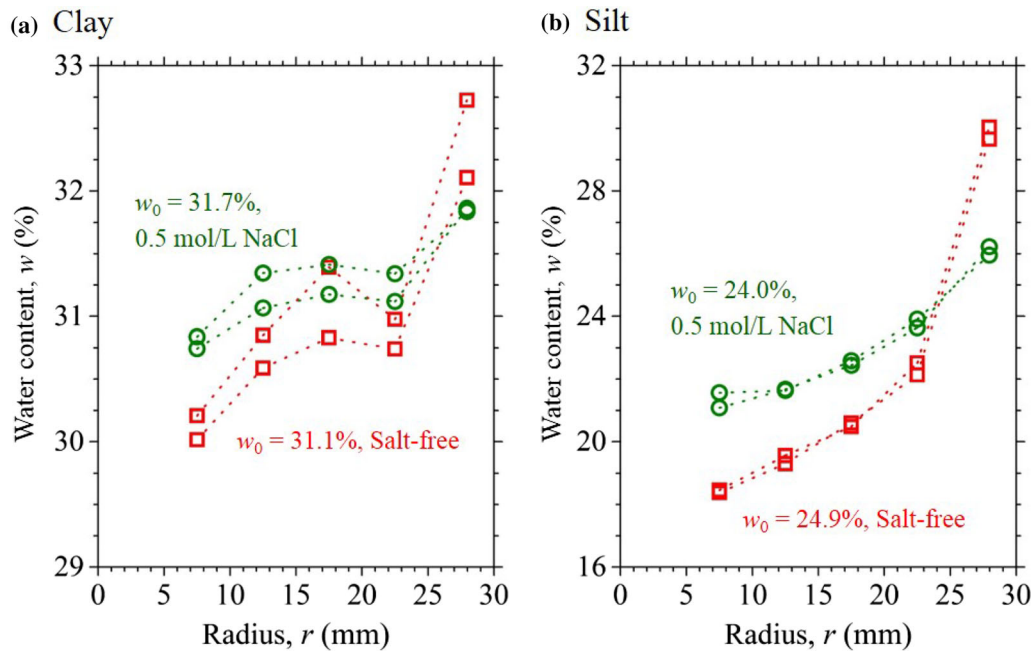
Fig. 7 Effect of salt on water redistribution

migration and frost heave. The mechanism for the effect of salt on water migration will be discussed in Sect. 4.

3.2 Results of frost heave test

Figure 8 shows the experimental results of frost heave tests. The top temperature gradually decreases to about − 3 °C and − 6 °C for salt-free and salt-bearing soils,

respectively. The lower temperature was adopted to compensate for the salt-induced freezing point depression. The bottom temperature was about 3 °C for all tests. Frost heave occurred evidently in the salt-free clay and silt, occurred slightly in the 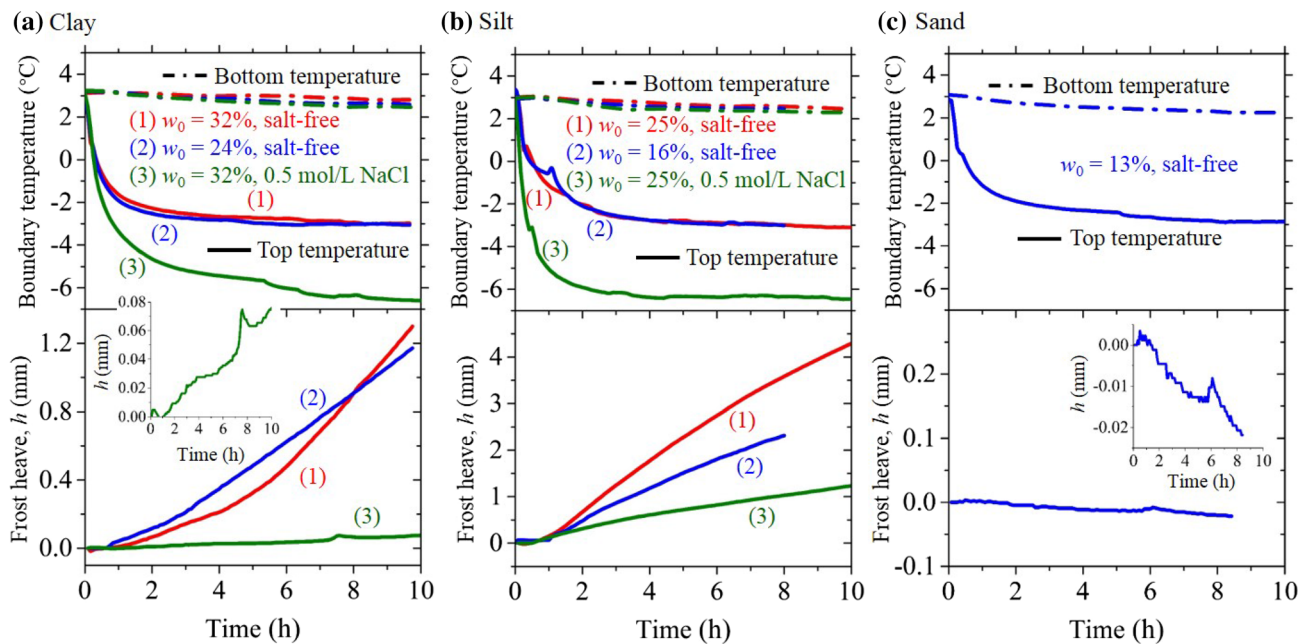salt-bearing clay, and did not occur in the sand. At the very early stage, the frozen zone may expand, but the unfrozen zone contracts (due to the negative pore water pressure and overburden pressure by the

Fig. 8 Evolution of boundary temperature and frost heave

frost heaving force); thus, the frost heave developed quite slowly. Frost heave increases faster after the unfrozen zone is sufficiently compressed. As the temperature tends to be steady, the thermal gradient and freezing rate decrease, decreasing the frost heave rate. Generally, the frost heave rate is higher in silt than in clay, higher in samples with higher initial water content, and higher in samples with lower salt concentration. These experimental results are qualitatively consistent with previous experimental studies [8, 10, 14, 20]. Notably, soil contracted very slightly instead of expanding in the sand test. As the bottom boundary is unfrozen and open to the external water source, the expansion of pore ice squeezes pore water down to outside the sand, limiting the in situ frost heave. Additionally, thermal shrinkage can cause the sand sample to contract when it undergoes cooling.

The water content along the height of the soil column was measured after the frost heave test (Figs. 9a-c). In salt-free clay, water content increases in the frozen (upper) zone and decreases in the unfrozen (lower) zone. A gradient of w built up in the unfrozen zone, driving water up to feed the growing ice lens (Fig. 9a). The highest water content occurred in the frozen zone near the freezing front, and the lowest water content occurred in the unfrozen zone near the freezing front. In the salt-bearing clay sample, the distribution of water changed slightly relative to the initial water content. In the silt with high initial water content ($w_0 = 25\%$), water content increased in the frozen zone and reduced in the unfrozen zone. However, in the silt with low initial water content ($w_0 = 16\%$), water content increased in both frozen and unfrozen zones. The increase in water content in the unfrozen silt is caused by the capillary pressure that sucks water from external water sources. Different from the clay situation, water distributes uniformly in the unfrozen zone. The difference in water content distribution between clay and silt is due to the difference between their hydraulic conductivities. Clay has a low hydraulic conductivity so a higher water content gradient is required to drive water to migrate. In contrast, silt has a much higher hydraulic conductivity, so the water content gradient is very low. In the sand, water content increases from top to bottom. Since cryogenic suction is negligible and capillary pressure plays a dominant role in the sand, water was sucked into the unsaturated sand and water content increased from top to bottom to balance the gravitational potential.

Figures 9d–f shows the images of the tested sample. In the clay sample, a network of ice lenses forms in the frozen zone, and the main ice lens occurs near the freezing front (Fig. 9d). In the silt sample, the frozen zone seems to be a whole entity and only one ice lens is visible near the freezing front (Fig. 9e). In the sand sample, no ice lens could be seen (Fig. 9f).

4 Model of radial freezing-induced water redistribution

4.1 Heat and water transfers at freezing front

During radial freezing, the sample center is the symmetric axis, and the freezing front is a contracting circle, as shown in Fig. 10. The inside of the freezing front is unfrozen, while the outside is frozen. Since the sample center is of zero heat flux, the temperature in the unfrozen zone would quickly drop to close to the freezing point. Therefore, shortly after the start of freezing, the latent heat of icing at the freezing front is mainly balanced by the heat flux through the frozen zone, as assumed in the derivation for the Stefan equation (Supporting information in reference [18]):

$$\lambda \frac{T_0 - T_c}{\delta_f} = L \rho \, \theta_0 \frac{d\delta_f}{dt} \tag{1}$$

where λ is the thermal conductivity; T_0 and T_c are the soil freezing point and boundary temperature, respectively; δ_f is the thickness of the frozen zone (annulus); L is the latent heat released by unit mass of water; ρ is the density of water; θ_0 is the initial volumetric water content; t is the time. In Eq. (1), the unfrozen water content and water migration were ignored. Although simplified, it still captures the primary characteristic of energy conservation in radial solidification.

At the initial state, $t = 0$, and $\delta_f = 0$. Thus, solving Eq. (1) with the initial condition yields:

$$\delta_f = \sqrt{\frac{2 \lambda (T_0 - T_c) t}{L \rho \, \theta_0}} \tag{2}$$

Eq. (2) is the Stefan equation, which is widely used to estimate the frost depth for ground [18, 34].

The freezing rate, V_f, is defined as the increasing rate of frozen thickness, i.e., $V_f = d\delta_f/dt$. From Eq. (2), one can easily obtain
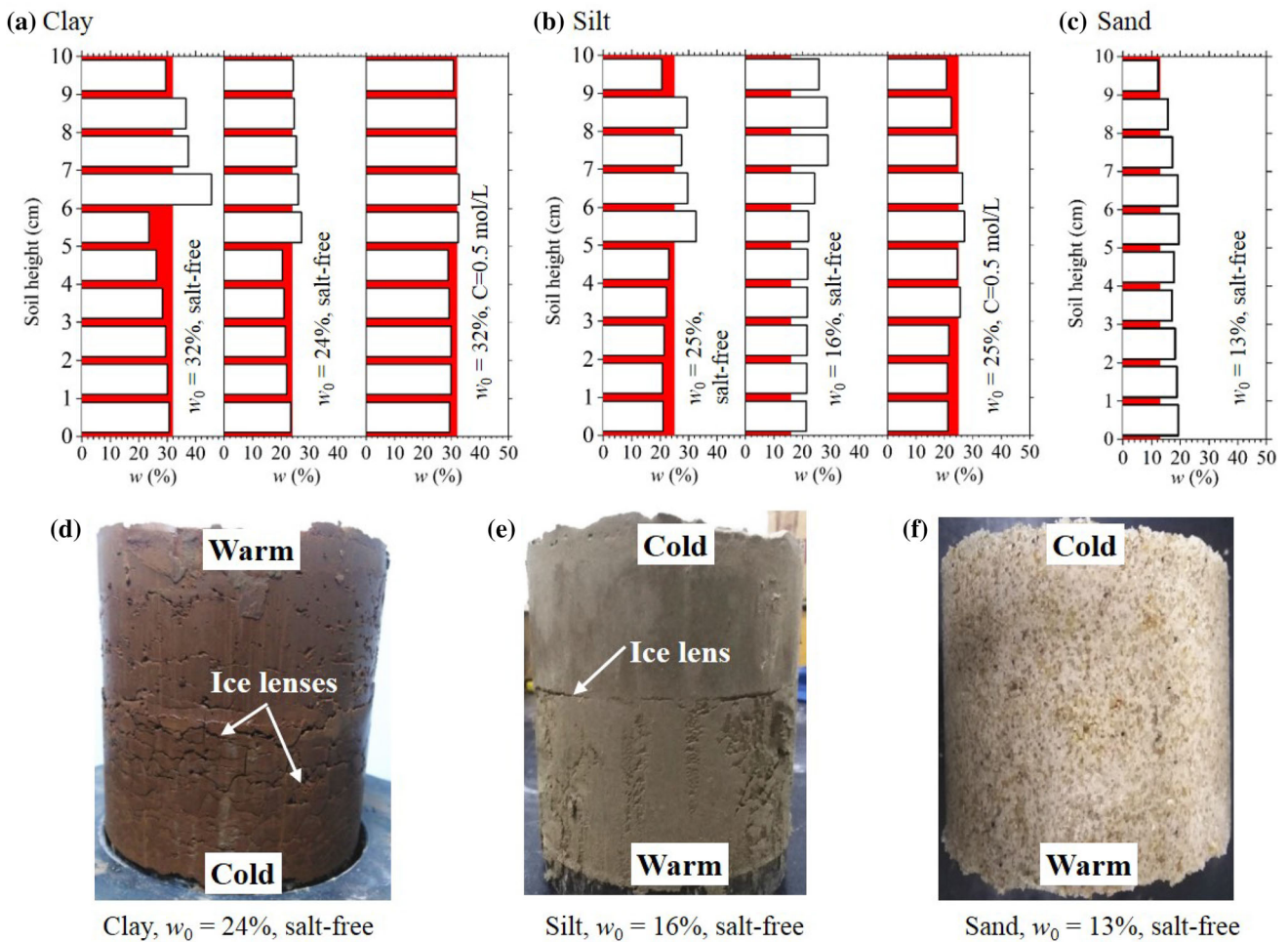
$$V_f = \frac{\lambda (T_0 - T_c)}{\delta_f L \rho \, \theta_0} \tag{3}$$

According to the Darcy's law, the volumetric water flux into the frozen zone is given by

$$V_w = -\frac{k}{\rho \, g} \nabla p_w \tag{4}$$

where k is the hydraulic conductivity of frozen soil at freezing front; g is the gravitational acceleration; p_w is the pore water pressure. The hydraulic conductivity k is highly influenced by the water and ice content. Taylor and Luthin (1978) introduced a resistance factor I to express the soil water diffusivity in the frozen soil. In this study, we assume

(a) Clay

(b) Silt

(c) Sand

Clay, $w_0 = 24\%$, salt-free

Silt, $w_0 = 16\%$, salt-free

Sand, $w_0 = 13\%$, salt-free

Fig. 9 Water redistribution of (**a**–**c**) and images (**d**–**f**) of samples after frost heaving tests. The white bars in (**a**–**c**) represent the water content, and the red areas represent the initial water content. The clay sample (**d**) was upside down when it was photographed
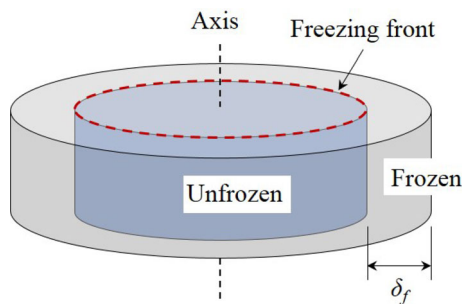
Fig. 10 Schematic of radial freezing

a similar factor I to relate the hydraulic conductivities between the unfrozen and frozen soil near the freezing front as follows:

$$k = \frac{k_0(\theta_u/\theta_s)^b}{I} \tag{5}$$

where k_0 is the hydraulic conductivity of saturated unfrozen soil; θ_u is the volumetric water content of unfrozen soil

at the freezing front; θ_s is the saturated water content; b is a parameter that expresses the decay of hydraulic conductivity in unsaturated soil. The resistance factor I express the effect of ice on the depression of hydraulic conductivity in frozen soil.

According to the generalized Clapeyron equation [47], pore water pressure is related to temperature as follows:

$$\eta(T_m - T) = \beta p_i - p_w + cRT \tag{6}$$

where η ($\approx$ 1.22 MPa/K) and β($\approx$ 1.09) are constants; T_m(= 273.15 K) is the freezing point of pure ice; p_i is the ice pressure; cRT is the osmotic pressure.

Under the condition of zero ice pressure and zero osmotic pressure, Eq. (6) gives

$$\nabla p_w = \eta \nabla T = \eta \frac{T_c - T_0}{\delta_f} \tag{7}$$

According to Eqs. (4), (5), and (7), the water flux is

$$V_w = \frac{k_0 (\theta_u/\theta_s)^b \eta (T_0 - T_c)}{I \rho g \, \delta_f} \tag{8}$$

During the radial freezing, the migrated water flux is assumed to freeze in a very narrow zone behind the freezing front. In an infinitesimal duration, Δt, the freezing front contracts, and the volume of frozen zone increases by $SV_f\Delta t$, where S is the lateral area of the cylinder covered by the freezing front (Fig. 10). The volume of the migrated water is $SV_w\Delta t$. The migrated water is stored in the expanded frozen zone, increasing water content by $D = SV_w\Delta t/SV_f \Delta t = V_w /V_f$, at the freezing front. Considering the expression of V_w and V_f (Eqs. 3 and 8), one could obtain

$$D = \frac{k_0 (\theta_u/\theta_s)^b \eta L \theta_0}{I g \lambda} = D_0 (\theta_u/\theta_s)^b \tag{9a}$$

where

$$D_0 = \frac{k_0 \eta L \theta_0}{I g \lambda} \tag{9b}$$

Eq. (8) shows that the velocity of water migration increases with the lowing boundary temperature T_c. However, T_c is eliminated in the expression of D (Eq. 9a), indicating that the increase in the water content is independent of the boundary temperature. This is validated by the results of the freezing ring test on silt with various boundary temperatures (Fig. 5b). This is different from the unidirectional freezing test, where the boundary temperature significantly impacts water redistribution and frost heave: the lower the boundary temperature is, the more severe the water migration occurs and frost heave develops [20].

The volumetric water content of the frozen zone at the freezing front, θ_f, is as follows:

$$\theta_f = \theta_u + D \tag{10}$$

4.2 Conservation of water content

Figures 11a–c show the evolution of water content distribution in the frozen and unfrozen zones during the freezing ring test. The origin represents the sample center, and r_f denotes the radius of the freezing front. The water in the unfrozen zone is sucked to the freezing front, forming a gradient of water content inside of the freezing front. The characteristic of water content distribution in the unfrozen zone is similar to the results of unidirectional freezing tests on salt-free clays (Fig. 9a). At the early stage of freezing, as the freezing rate is fast, the nonuniformly distributed water content does not have sufficient time to achieve equilibrium, and the gradient of water content is high (Fig. 11a). At a location away from the freezing front, the water content recovers to initial volumetric water content θ_0. It means that there is a transitional layer, where water content varies from

θ_u to θ_0. The thickness of the transitional layer is denoted by δ. Beyond the transitional layer is the undisturbed zone expressed by $r < r_f–\delta$. As freezing continues, the freezing rate slows down and more unfrozen zone is influenced by water migration. Thus, the transitional layer thickens, i.e., δ increases (Fig. 11b). Once the transitional layer extends to the sample center, all unfrozen zone is disturbed and water content decreases (Fig. 11c).

For practical purposes, the water distribution in the transitional layer is assumed to be constant (Fig. 11a'–c'). When $\delta < r_f$ (Fig. 11a'–b'), the water content in the unfrozen zone is as follows:

$$\theta = \begin{cases} \theta_0, & r < r_f - \delta \\ \theta_u, & r_f - \delta < r \le r_f \end{cases} \tag{11a}$$

However, when $\delta \ge r_f$ (Fig. 11c'), the entire unfrozen zone is disturbed, and the water content is as follows:

$$\theta = \theta_u, \quad r < r_f \tag{11b}$$

The thickness of the transitional layer is highly influenced by the freezing rate. During faster freezing, the freezing front moves fast, and water in the inner zone does not have sufficient time to migrate outward. Thus, only a relatively narrow transitional layer is disturbed near the freezing front. Through the first approximation, it is assumed that $\delta \propto 1/V_f$. From Eq. (3), one can obtain that $1/V_f \propto \delta_f$. Thus, the thickness of the transitional layer can be assumed as

$$\delta = m \, \delta_f = m \, (R - r_f) \tag{12}$$

where m is the constant of proportionality; R is the radius of the sample; $\delta_f = R–r_f$ is the thickness of the frozen zone.

In this study, the water content in the frozen zone refers to the total water content. The volumes of water in the undisturbed zone, transitional layer, and frozen zone are denoted as Q_{u1}, Q_{u2}, and Q_f, respectively. Integrating θ in these zones gives

$$Q_{u1} = \theta_0 \pi (r_f - \delta)^2 l \tag{13a}$$

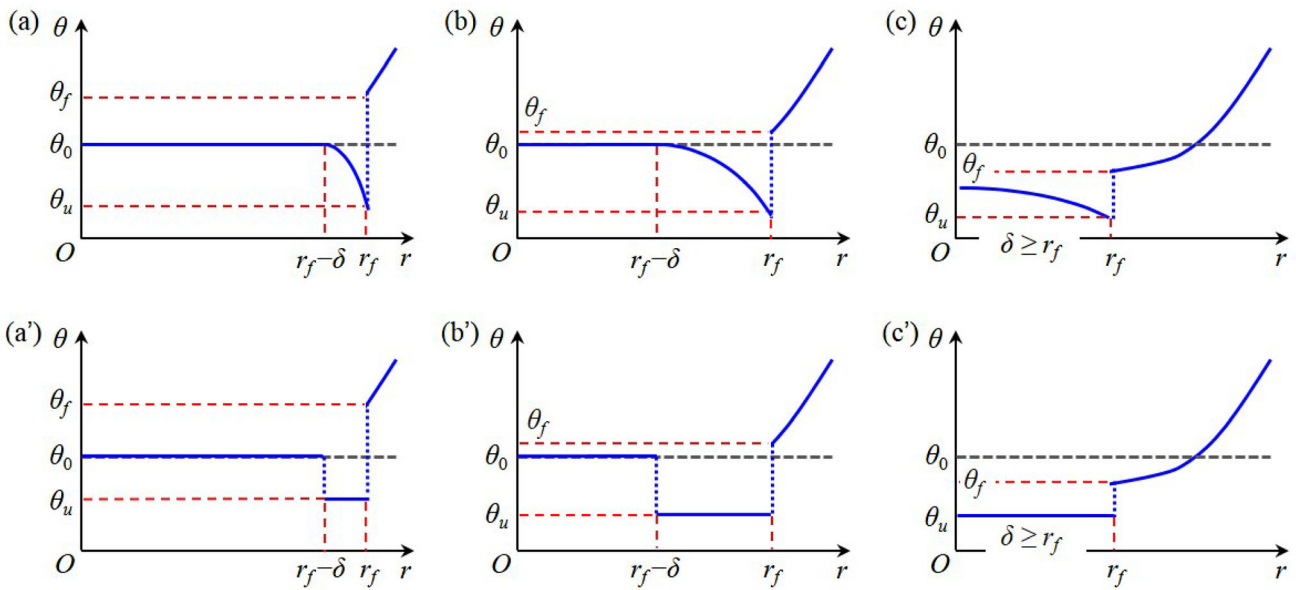$$Q_{u2} = \theta_u \pi [r_f^2 - (r_f - \delta)^2] \, l \tag{13b}$$

$$Q_f = \int_{r_f}^{R} \theta \cdot 2\pi r l \cdot \mathrm{d}r \tag{13c}$$

where l is the height of the sample.

Substituting Eq. (12) into Eqs. (13) and taking their differentials yields

$$\frac{\mathrm{d}Q_{u1}}{\pi l} = \theta_0 (2A_1 r_f + B_1) \mathrm{d}r_f \tag{14a}$$

$$\frac{\mathrm{d}Q_{u2}}{\pi l} = (A_2 r_f^2 + B_2 r_f + C_2) \mathrm{d}\theta_u + \theta_u (2A_2 r_f + B_2) \mathrm{d}r_f \tag{14b}$$

Fig. 11 Schematic of water redistribution during soil freezing. (**a–c**) A gradient of water content characterizes the transitional layer from $r_f - \delta$ to r_f. (**a'–c'**) The water content in the transitional layer is assumed to be constant

$$\frac{dQ_f}{\pi l} = -2r_f\theta_f dr_f = -2r_f[\theta_u + D_0(\theta_u/\theta_s)^b]dr_f \quad (14c)$$

where

$$A_1 = (1+m)^2; \quad B_1 = -2mR(m+1) \quad (15a)$$

$$A_2 = -m(m+2); \quad B_2 = 2mR(m+1); \quad C_2 = -m^2R^2 \quad (15b)$$

In the derivation of Eq. (14c), Eqs. (9a) and (10) are used.

The conservation of water content requires $d(Q_{u1} + Q_{u2} + Q_f) = 0$. Thus, uniting Eqs. (14a–c) yields:

$$\frac{d\theta_u}{dr_f} = \frac{2r_f[\theta_u + D_0(\theta_u/\theta_s)^b] - \theta_0(2A_1r_f + B_1) - \theta_u(2A_2r_f + B_2)}{A_2r_f^2 + B_2r_f + C_2} \quad (16)$$

When $\delta = r_f$, the transitional layer reaches the center, and the undisturbed zone disappears. In this case, the total volume of water in the unfrozen zone is $Q_u = \pi r_f^2 l\theta_u$. Thus, the differential form is

$$\frac{dQ_u}{\pi l} = r_f^2 d\theta_u + 2\theta_u r_f dr_f \quad (17)$$

The conservation of water content requires $d(Q_u + Q_f) = 0$, from which one can obtain

$$\frac{d\theta_u}{dr_f} = \frac{2D_0(\theta_u/\theta_s)^b}{r_f} \quad (18)$$

Eqs. (16) and (18) can be summarized as follows:

$$\frac{d\theta_u}{dr_f} = y(r_f, \theta_u) \quad (19a)$$

where

$$y(r_f, \theta_u)$$

$$= \begin{cases} \dfrac{2r_f[\theta_u + D_0(\theta_u/\theta_s)^b] - \theta_0(2A_1r_f + B_1) - \theta_u(2A_2r_f + B_2)}{A_2r_f^2 + B_2r_f + C_2}, \\ \qquad\qquad r_f > \delta \\ \dfrac{2D_0(\theta_u/\theta_s)^b}{r_f}, \\ \qquad\qquad r_f \le \delta \end{cases} \quad (19b)$$

Eq. (19) implies that the water content tends to negative infinity when r_f tends to zero, which is unrealistic. When the water content in the sample center ($r_f = 0$) is too low, the suction becomes extremely high so that it is impossible to attract the water there outward. Therefore, Eq. (19) only applies when the radius does not approach the sample center.

At the initial condition, $r_f = R$, and $\theta_u = \theta_0$. However, if $r_f = R$, $A_2r_f^2 + A_2r_f + C_2 = 0$, and $y(r_f, \theta_u)$ would be infinity. To avoid this singularity, a factor ε is introduced to the initial condition:

$$\theta_u = \theta_0, \quad \text{when } r_f = \varepsilon R \quad (20)$$

When ε tends to 1, Eq. (20) tends to the real initial condition; however, $y(r_f, \theta_u)$ tends to singularity. Thus, a value of slightly less than 1 is reasonable for practical purposes. In this study, ε is set as 0.95.

Eq. (19a) is a nonlinear ordinary differential equation, which can be easily solved using numerical methods. Solving Eq. (19a) with the initial condition Eq. (20), one can obtain the volumetric water content of unfrozen zone at the freezing front $\theta_u(r_f)$. Using Eq. (10), we can obtain the volumetric water content of frozen zone at the freezing front $\theta_f(r_f) = \theta_u(r_f) + D$. Since the hydraulic conductivity is extremely low in the frozen zone, the water content of frozen zone does not change with time. Thus, the water content at the freezing front $\theta_f(r_f)$ gives the water content of the frozen zone at any radius $\theta(r)$ when the freezing front is moving (Fig. 11). The gravitational water content and volumetric water content can be converted into each other $w(r) = \theta(r)\rho_d/\rho$. Consequently, the redistribution of the gravitational water content after freezing is

$$w(r) = \frac{\rho}{\rho_d}\left[\theta_u(r_f) + D\right] \qquad (21)$$

where ρ_d and ρ are the dry density of soil and water density, respectively.

As mentioned above, when the freezing front tends to the sample center the water content decreases infinitely, which is unrealistic. The water content in the unfrozen zone is hard to migrate if the water content is very low so that the water content in the sample center would not decrease infinitely. In this study, water redistribution was calculated to the least radius of 5 mm.

5 Discussion

5.1 Characteristics of water redistribution

The water redistribution curve for the freezing ring test can be obtained by applying the water redistribution model with parameters presented in Table 3. Figure 12 compares

Table 3 Model parameters for radial freezing-induced water redistribution

| Soil type	w_0 (%)	w_s (%)	D_0	b	m	Remark
Clay	31.1	32.5	0.02	2	0.5	$\rho_d = 1.45$ g/cm^3
	31.2	32.5	0.005	2	0.5	Salt-bearing; $\rho_d = 1.45$ g/cm^3
	23.6	26.0	0.01	2	0.5	
Silt	24.9	25.7	0.25	5	8	
	24.9	25.7	0.25	5	8	$R = 25$ mm
	24.0	25.7	0.10	5	8	Salt-bearing
	15.7	25.7	0.25	5	8	

$\rho_d = 1.60$ g/cm^3, $R = 30.9$ mm, and soil is salt-free if without remark; θ_0 and θ_s are converted from w_0 and w_s

the experimental and modeled water redistribution. Although there is some disagreement, the model captures the main characteristics of water redistribution. In clay samples (Fig. 11a, b), water increases significantly near the boundary. In the intermediate zone, the water content changes slightly. As the freezing propagates to the inner zone, the water content decreases again. As a comparison, in the silt samples (Fig. 11c, d), the water content decreases monotonously from the outer to the inner zone without inflection.

The effect of salt on the water redistribution curve is modeled by lowering the parameter D_0, which describes the abrupt increase in the water content at the freezing front. D_0 is mainly determined by the migrated water flux (or water migration velocity) V_w. During freezing, salt can be excluded from the freezing front and accumulates in the unfrozen zone in front of the freezing front, thus, developing a salt concentration gradient in this zone. Due to the salt-induced freezing point depression, a freezing point gradient can also be developed in front of the freezing front: the closer to the freezing front, the lower the freezing point. At the freezing front, soil temperature is equal to the freezing point and the freezing front is in equilibrium. However, when it goes to the unfrozen zone away from the freezing front, both soil temperature and freezing point increase. If freezing point gradient is greater than soil temperature gradient in this unfrozen zone, the soil temperature is lower than the freezing point and the unfrozen zone is supercooled. The phenomenon of soil supercooling induced by salt concentration gradient in unfrozen zone is called constitutional supercooling [29, 42]. The constitutional supercooling is an unsteady state, since the soil particles, pore water, and salt, could be engulfed together by the moving freezing front. In this situation, the water migration and ice segregation are highly weakened, thus, reducing D_0. Clay has smaller pores than silt; therefore, it is harder for salt to diffuse in clay than in silt. The gradient of salt concentration, the gradient of freezing point, and the constitutional supercooling in clay are greater than in silt. Thus, salt has a more significant impact on the water redistribution in clay than silt (Figs. 11a & c).

The boundary radius is $R = 30.9$ mm for all samples in the freezing ring test. To model the inner zone surrounded by the plastic film ring at a radius of 25 mm (Fig. 5a), we calculated the water redistribution curve by changing the boundary radius to $R = 25$ mm (curve 3 in Fig. 12c). Curves (1) and (3) in Fig. 12c were obtained using the same model parameters except for the boundary radius. These two curves show that the water content differs in the outer zone but converges in the inner zone, indicating that the sample size has less impact on the water content in the inner zone. In the test on clay with lower initial water content (Fig. 12b), parameter D_0 was reduced from 0.02 to
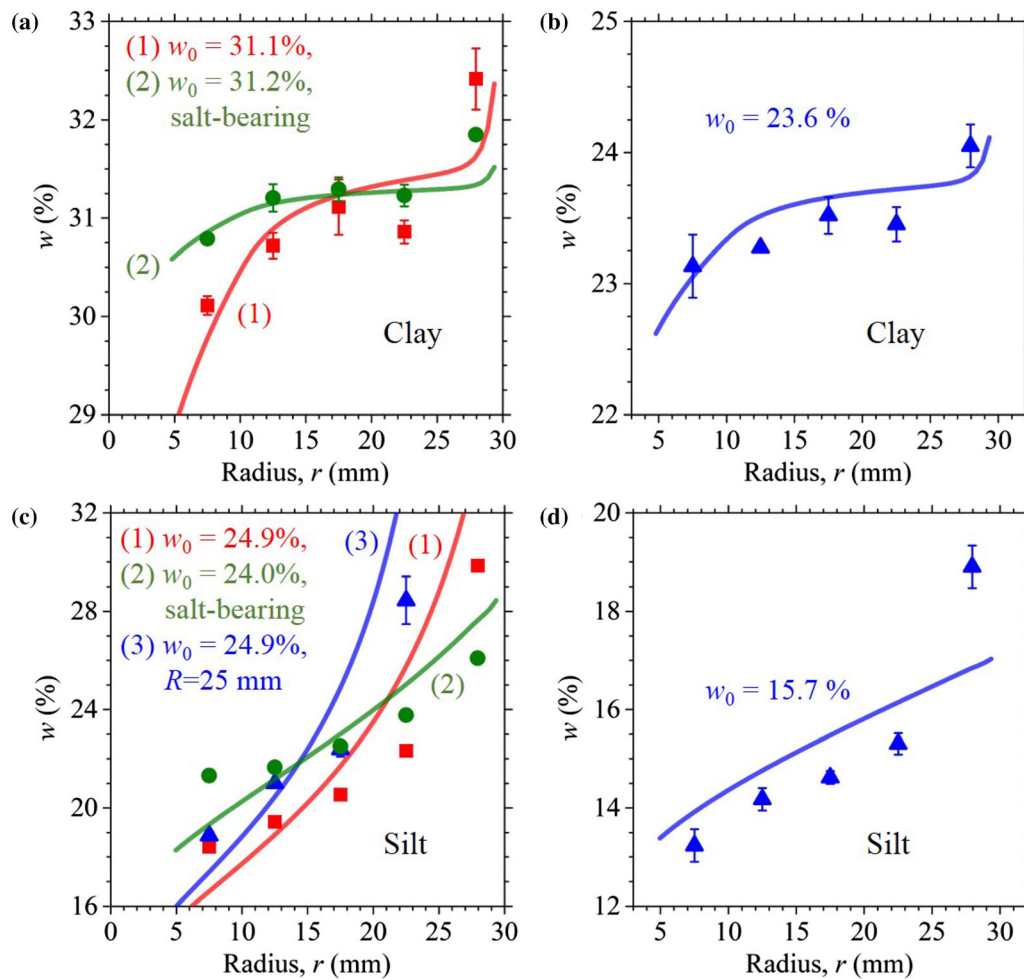
Fig. 12 Experimental (points) and modeled (curves) results of water redistribution after radial freezing. In (**a**) and (**c**), the points marked by square, circle, and triangle correspond to the curves marked (1), (2), and (3), respectively

0.01 due to its higher compactness. The silt sample with lower initial water content has the same soil properties as the sample with higher initial water content; thus, it is modeled with the same D_0 (Fig. 12d). As expressed in Eq. (8), the water migration flux is also influenced by the unfrozen water content. Therefore, lower initial water content results in lower water migration and less significant water redistribution.

5.2 Parameter sensitivity

The parameters D_0, m, and b represent the water transfer capability, thickness of the transitional layer, and decay of hydraulic conductivity with decreasing water content, respectively. It is helpful to get insight into the water migration characteristics by analyzing the parameter sensitivity. Figure 13 shows the modeled results with variable model parameters D_0, m, and b. The higher D_0 means higher water transfer capability, resulting in higher nonuniformity of water content (Fig. 13a). The parameter

m expresses the expansion rate of the transitional layer at a given freezing rate. It has a significant impact on the shape of the redistribution curve. At a low value of m, the water redistribution curve is relatively flat in the intermediate zone (Fig. 13b). In high-permeability soil, the water migrates easily so that the transitional layer expands fast. In contrast, the transitional layer expands slowly in the low-permeability soil. This coincides with the fact that the relatively flat section occurred in the water redistribution curve of clay samples instead of silt samples (Fig. 12). The parameter b expresses the decay of hydraulic conductivity with desaturation. Figure 13c shows that the variation of b has an insignificant impact on the water redistribution curve in the outer zone. A lower value of b means less decay in the hydraulic conductivity so that water migrates more easily due to cryogenic suction, leading to lower water content in the inner zone.
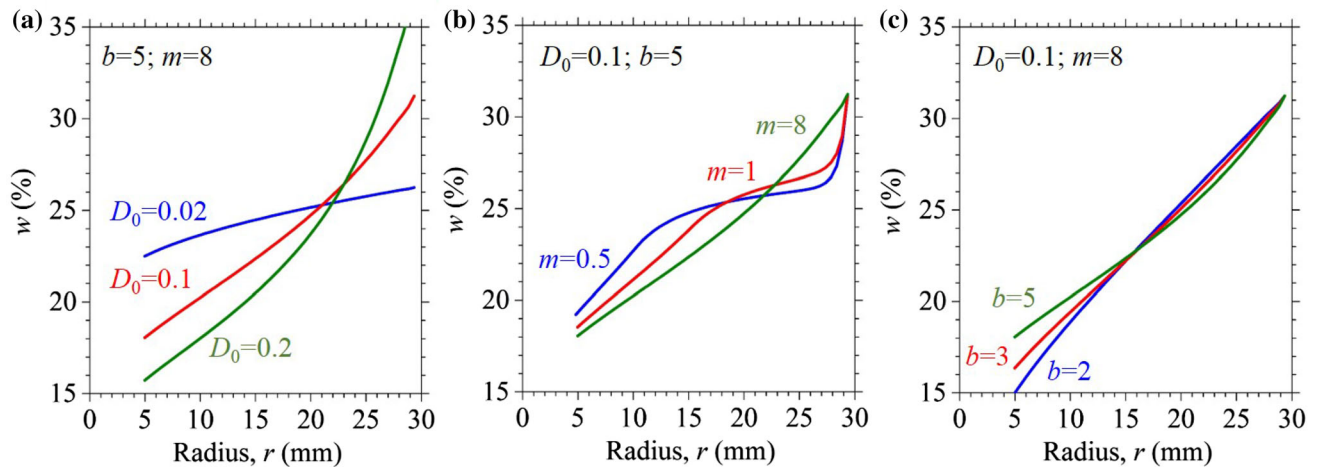
Fig. 13 Sensitivity of water redistribution curve to model parameters. Other parameters used for calculation are $\rho_d = 1.6$ g/cm^3, $w_0 = 25\%$, and saturated water content $w_s = 25\%$

5.3 Assessing frost susceptibility of soils

Two possible indices can be used to assess frost susceptibility: frost heave amount and frost heave rate. The frost heave amount obtained in laboratory depends on the testing time and usually does not indicate the real frost heave amount in field. Thus, it is not easy to classify frost susceptibility by frost heave amount in a wide range of applications. In contrast, the maximum frost heave rate can easily be determined and is less dependent on the testing time. In this study, we choose the maximum frost heave rate V_h, within 8 h after frost heave initiates, as the index of frost susceptibility. This is similar to the 8-h frost heave rate adopted by ASTM International [3] for assessing frost susceptibility.

The water redistribution curve obtained from the freezing ring test shows the nonuniformity of water content caused by water migration during freezing. Intuitively, the maximum difference in water content between the outermost ($r = 28.0$) and innermost ($r = 7.5$) layers, denoted as Δw_{oi}, could be used as the index for water nonuniformity (Fig. 1c). Alternatively, we can choose the increase in water content at the outermost layer relative to the initial water content (denoted as Δw_{o0}) to characterize water migration. To obtain Δw_{oi}, the sample should be cut layer by layer to obtain the innermost layer. In contrast, to obtain Δw_{o0}, the soil needs to be cut only once by the largest cutting ring. Thus, Δw_{o0} is easier to obtain than Δw_{oi}, and this simplicity may be time-saving in large projects.

Figure 14 shows the variation of water nonuniformity (Δw_{oi} and Δw_{o0}) and maximum frost heave rate (V_h). The qualitative trends are quite similar. Water migration and frost heave are the most severe in silt, lower in clay, and negligible in sand; in both silt and clay, higher initial water content would improve water migration and frost heave,

but salt concentration depresses them. Although Δw_{oi} is about twice as much as Δw_{o0} (Fig. 13a, b), they have almost the same trends. As mentioned before, Δw_{o0} is easier to measure than Δw_{oi}. Thus, Δw_{o0} is suggested as the water nonuniformity index to assess frost susceptibility.

The maximum frost heave rate V_h is plotted against Δw_{o0}, as shown in Fig. 15, from which an overall linear relation can be concluded. The correlation between V_h and Δw_{o0} confirms that the freezing ring test provides an easy way to assess frost susceptibility of soils. The classification of frost susceptibility by the 8-h frost heave rate suggested by ASTM was employed in the classification by V_h in this study. According to the criteria, frost susceptibility is classified into *Negligible*, *Very low*, *Low*, *Medium*, *High*, and *Very high*, depending on V_h (Fig. 16). Additionally, from the relationship between V_h and Δw_{o0}, the classification by V_h can be converted to a classification by Δw_{o0}, shown as the vertical lines in the classification chart. V_h and Δw_{o0} criteria agree in the light blue zones in the classification chart, showing that the frost susceptibility is *High* for salt-free silt, *Medium* for salt-bearing silt, and clay with high initial water content, and *Negligible* for sand. However, disagreement between V_h and Δw_{o0} criteria (white zones in the classification chart) occurs in the other clay samples. In the clay with lower initial water content, frost susceptibility is *Low* according to V_h criteria but *Very low* according to Δw_{o0} criteria. In the salt-bearing clay, frost susceptibility is *Negligible* according to V_h criteria but *Very low* according to Δw_{o0} criteria. This disagreement implies the limitation of the freezing ring test in assessing soils that is insensitive to frost heave. This limitation could be overcome by more laboratory tests and field monitoring, from which more sophisticated classification criteria can be developed.
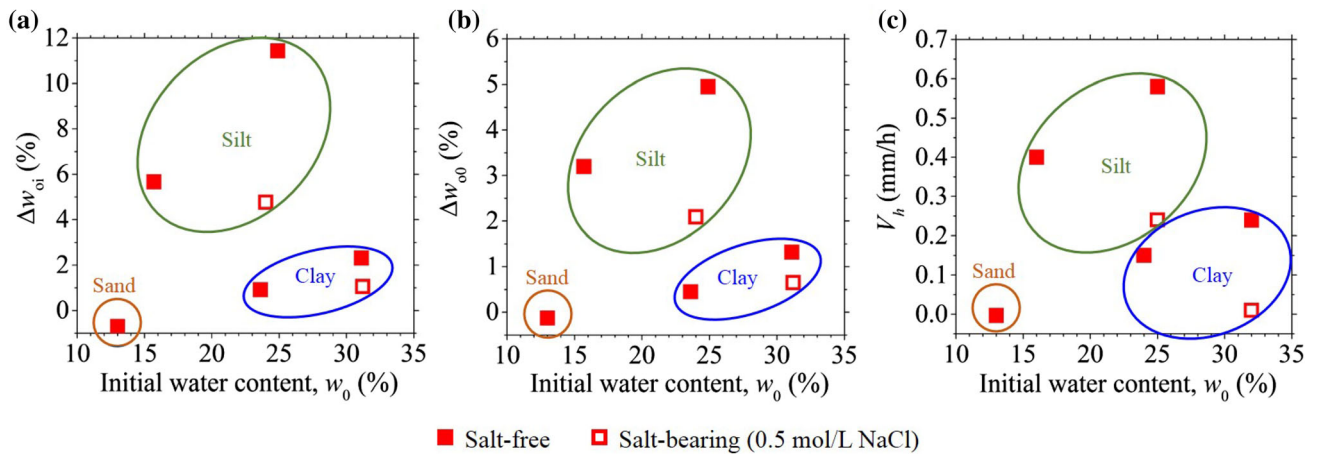
Fig. 14 Variation of water nonuniformity (a. Δw_{oi} and b. Δw_{o0}) and maximum frost heave rate (c. V_h)
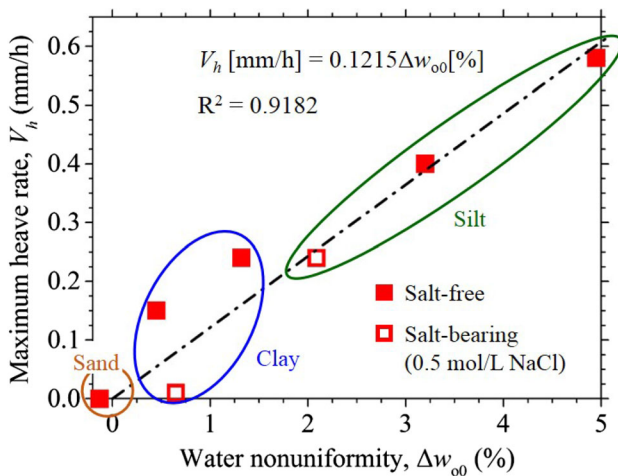

Fig. 15 Relationship between maximum frost heave rate and water nonuniformity

Fig. 16 Classification chart of frost susceptibility. VH, H, M, L, VL, and N denote *Very high*, *High*, *Medium*, *Low*, *Very low*, and *Negligible*, respectively. The data points are the same as those in Fig. 15

6 Conclusions

This study conducted a series of freezing ring tests and traditional frost heave tests, considering the effects of soil type, initial water content, and salt concentration. In the freezing ring test, water migration due to cryogenic suction increases the water content in the outer zone but decreases in the inner zone. The water redistribution during freezing ring tests is independent of the boundary temperature. In the unidirectional freezing tests, water migration results in frost heave. Water migration and frost heave are the most significant in silt, lower in clay, and negligible in sand. Higher initial water content would enhance water migration and frost heave, but salt could depress them.

A theoretical model is presented to characterize the water redistribution during freezing ring tests. The model verified that the water redistribution curve is ind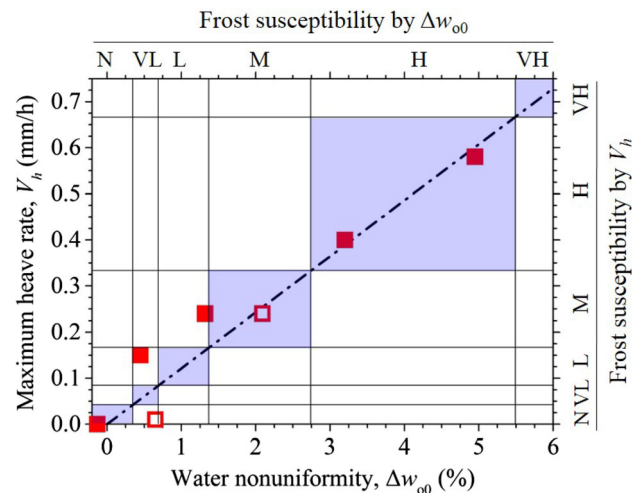ependent of boundary temperature. According to the model, a transitional layer forms in the unfrozen zone, where the water content varies significantly. The transitional layer influences the shape of the water redistribution curve. In clay, the transitional layer is thin due to its low hydraulic water conductivity, causing an inflection on the water redistribution curve. In contrast, the water content varies without inflection in silt. Salt is excluded from the freezing front so that a gradient of salt concentration builds up in the unfrozen zone, inducing the constitutional supercooling and depressing water migration.

Water nonuniformity indices are introduced to express the water migration capability in freezing ring tests. The maximum frost heave rate is adopted to express the frost susceptibility. A good correlation between water nonuniformity and frost heave rate indicates that the freezing ring test is an easy way to assess frost susceptibility of soils.

The frost susceptibility can be classified according to the maximum frost heave rate or water nonuniformity. The frost susceptibility is *High* in salt-free silt, *Medium* in salt-bearing silt and clay with high initial water content, and *Negligible* in sand. Disagreement between the classification criterion by water nonuniformity and frost heave rate occurred in the soil with low frost susceptibility.

References

1. Akagawa S, Hori M, Sugawara J (2017) Frost heaving in ballast railway tracks. Proced Eng 189:547–553. https://doi.org/10.1016/j.proeng.2017.05.087

2. Armstrong MD, Csathy TI (1963) Frost design practice in Canada. Highw Res Rec 33:170–201

3. ASTM Standard D5918–13e1 (2013) Standard Test Methods for Frost Heave and Thaw Weakening Susceptibility of Soils. ASTM International, West Conshohocken. https://www.astm.org/Standards/D5918.htm

4. Bai R, Lai Y, Pei W, Zhang M (2020) Investigation on frost heave of saturated–unsaturated soils. Acta Geotech 15:3295–3306. https://doi.org/10.1007/s11440-020-00952-6

5. Beskow G (1935) Soil freezing and frost heaving with special application to roads and railways. Swedish Geotechnical Society, Stockholm

6. Bonnard D, Recordon E (1958) Road foundations: Problems of bearing capacity and frost resistance. Strasse und Verkehr, 44:311–381. (CREEL Translation from French)

7. Carter M, Bentley SP (2016) Frost susceptibility. Soil properties and their correlations, 2nd edn. Wiley, New York, pp 164–174

8. Cary JW (1987) A new method for calculating frost heave including solute effects. Water Resour Res 23:1620–1624. https://doi.org/10.1029/WR023i008p01620

9. Chamberlain EJ (1981) Frost Susceptibility of Soil: Review of Index Tests. US Army Corps of Engineers, CRREL, Hanover, New Hampshire.

10. Chamberlain EJ (1983) Frost heave of saline soils. In: Péwé TL, Brown J (ed) Proceedings of 4th International Conference on Permafrost, National Academy Press, Washington, D.C. 121–126.

11. Everett DH (1961) The thermodynamics of frost damage to porous solids. Trans Faraday Soc 57:1541–1551. https://doi.org/10.1039/tf9615701541

12. Fowler AC, Krantz WB (1994) A generalized secondary frost heave model. SIAM J Appl Math 54:1650–1675. https://doi.org/10.1137/S0036139993252554

13. Ke Y, Que Y, Fu Y, Jiang Z, Easa S, Chen Y (2021) In situ frost-heaving characteristics of shallow layer of soil slopes in intermittently frozen region based on PFC3D. Adv Civ Eng 2021:6646514. https://doi.org/10.1155/2021/6646514

14. Kinosita S (1979) Effects of initial soil-water conditions on frost heaving characteristics. Eng Geol 13:41–52. https://doi.org/10.1016/0013-7952(79)90019-X

15. Kjelstrup S, Ghoreishian Amiri SA, Loranger B, Gao H, Grimstad G (2021) Transport coefficients and pressure conditions for growth of ice lens in frozen soil. Acta Geotech 16:2231–2239. https://doi.org/10.1007/s11440-021-01158-0

16. Konrad J-M, Morgenstern NR (1981) The segregation potential of a freezing soil. Can Geotech J 18:482–491. https://doi.org/10.1139/t81-059

17. Konrad J-M, Morgenstern NR (1982) Prediction of frost heave in the laboratory during transient freezing. Can Geotech J 19:250–259. https://doi.org/10.1139/t82-032

18. Kurylyk BL, Hayashi M (2015) Improved Stefan equation correction factors to accommodate sensible heat storage during soil freezing or thawing. Permafrost Periglac 27:189–203. https://doi.org/10.1002/ppp.1865

19. Lackner R, Amon A, Lagger H (2005) Artificial ground freezing of fully saturated soil: thermal problem. J Eng Mech 131:211–220. https://doi.org/10.1061/(ASCE)0733-9399(2005)131:2(211)

20. Lai Y, Pei W, Zhang M, Zhou J (2014) Study on theory model of hydro-thermal–mechanical interaction process in saturated freezing silty soil. Int J Heat Mass Tran 78:805–819. https://doi.org/10.1016/j.ijheatmasstransfer.2014.07.035

21. Long X, Cen G, Cai L, Chen Y (2018) Model experiment of uneven frost heave of airport pavement structure on coarse-grained soils foundation. Constr Build Mater 188:372–380. https://doi.org/10.1016/j.conbuildmat.2018.08.100

22. Marwan A, Zhou M, Abdelrehim MZ, Meschke G (2016) Optimization of artificial ground freezing in tunneling in the presence of seepage flow. Comput Geotech 75:112–125. https://doi.org/10.1016/j.compgeo.2016.01.004

23. Miller RD (1972) Freezing and heaving of saturated and unsaturated soils. Highw Res Rec 393:1–11

24. Niu F, Zheng H, Li A (2020) The study of frost heave mechanism of high-speed railway foundation by field-monitored data and indoor verification experiment. Acta Geotech 15:581–593. https://doi.org/10.1007/s11440-018-0740-8

25. O'Neill K, Miller RD (1985) Exploration of a rigid ice model of frost heave. Water Resour Res 21:281–296. https://doi.org/10.1029/WR021i003p00281

26. Palmer AC, Williams PJ (2003) Frost heave and pipeline upheaval buckling. Can Geotech J 40:1033–1038. https://doi.org/10.1139/t03-044

27. Penner E, Ueda T (1977) Dependence of frost heaving on load application-Preliminary results. In: Proceedings of International Symposium on Frost Action in Soils. University of Lulea, Sweden, pp 92–101.

28. Peppin SSL, Style RW (2013) The physics of frost heave and ice-lens growth. Vadose Zone J 12(vzj2012):0049. https://doi.org/10.2136/vzj2012.0049

29. Peppin SSL (2020) Stability of ice lenses in saline soils. J Fluid Mech 886:A16. https://doi.org/10.1017/jfm.2019.1065

30. Pimentel E, Sres A, Anagnostou G (2012) Large-scale laboratory tests on artificial ground freezing under seepage-flow conditions. Géotechnique 62:227–241. https://doi.org/10.1680/geot.9.P.120

31. Rempel AW, Wettlaufer JS, Worster MG (2004) Premelting dynamics in a continuum model of frost heave. J Fluid Mech 498:227–244. https://doi.org/10.1017/S0022112003006761

32. Roe PG, Webster DC (1984) Specification for the TRRL Frost Heave Test. Transport and Road Research Laboratory, HMSO, London.

33. Sarsembayeva A, Collins PEF (2017) Evaluation of frost heave and moisture/chemical migration mechanisms in highway subsoil

using a laboratory simulation method. Cold Reg Sci Technol 133:26–35. https://doi.org/10.1016/j.coldregions.2016.10.003

34. Stefan J (1891) Über die Theorie der Eisbildung, insbesondere über die Eisbildung im Polarmee. Annals Phys Chem 42:269–286

35. Style RW, Peppin SSL (2012) The kinetics of ice-lens growth in porous media. J Fluid Mech 692:482–498. https://doi.org/10.1017/jfm.2011.545

36. Sweidan AH, Niggemann K, Heider Y, Ziegler M, Markert B (2021) Experimental study and numerical modeling of the thermo-hydro-mechanical processes in soil freezing with different frost penetration directions. Acta Geotech. https://link.springer.com/article/10.1007%2Fs11440-021-01191-z

37. Taber S (1930) The mechanics of frost heaving. J Geol 38:303–317

38. Teng J, Liu J, Zhang S, Sheng D (2020) Modelling frost heave in unsaturated coarse-grained soils. Acta Geotech 15:3307–3320. https://doi.org/10.1007/s11440-020-00956-2

39. Teng J, Shan F, He Z, Zhang S, Zhao G, Sheng D (2019) Experimental study of ice accumulation in unsaturated clean sand. Géotechnique 69:251–259. https://doi.org/10.1680/jgeot.17.P.208

40. US Army Corps of Engineers (1965) Soils and geology-pavement design for frost conditions. Department of the Army Technical Manual, TM5–818–2. US Army Corps of Engineers, Hanover, New Hampshire.

41. Wettlaufer JS, Worster MG, Wilen LA (1997) Premelting dynamics: geometry and interactions. J Phys Chem B 101:6137–6141

42. You J, Wang L, Wang Z, Li J, Wang J, Lin X, Huang W (2016) Interfacial undercooling in solidification of colloidal suspensions: analyses with quantitative measurements. Sci Rep 6:28434. https://doi.org/10.1038/srep28434(2016)

43. Zhou G-Q, Zhou Y, Hu K, Wang Y-J, Shang X-Y (2018) Separate-ice frost heave model for one-dimensional soil freezing process. Acta Geotech 13:207–217. https://doi.org/10.1007/s11440-017-0579-4

44. Zhou J, Wei C (2020) Ice lens induced interfacial hydraulic resistance in frost heave. Cold Reg Sci Technol 171:102964. https://doi.org/10.1016/j.coldregions.2019.102964

45. Zhou J, Wei C, Wei H, Tan L (2014) Experimental and theoretical characterization of frost heave and ice lenses. Cold Reg Sci Technol 104–105:76–87. https://doi.org/10.1016/j.coldregions.2014.05.002

46. Zhou J, Meng X, Wei C, Pei W (2020) Unified soil freezing characteristic for variably-saturated saline soils. Water Resour Res 56:e2019WR026648. https://doi.org/10.1029/2019WR026648

47. Zhou J, Wei C, Lai Y, Wei H, Tian H (2018) Application of the generalized clapeyron equation to freezing point depression and unfrozen water content. Water Resour Res 54:9412–9431. https://doi.org/10.1029/2018WR023221